Photodiagnosis and Photodynamic Therapy 25 (2019) 214–224

Contents lists available at ScienceDirect

Photodiagnosis and Photodynamic Therapy

journal homepage: www.elsevier.com/locate/pdpdt

# Benefits of hypericin transport and delivery by low- and high-density lipoproteins to cancer cells: From *in vitro* to *ex ovo*

Lenka Lenkavska[a], Ludmila Blascakova[b], Zuzana Jurasekova[a,b], Mariana Macajova[c], Boris Bilcik[c], Ivan Cavarga[c], Pavol Miskovsky[b], Veronika Huntosova[b,*]

[a] Department of Biophysics, Faculty of Science, P. J. Safarik University in Kosice, Jesenna 5, 041 54 Kosice, Slovakia
[b] Center for Interdisciplinary Biosciences, Technology and Innovation Park, P. J. Safarik University in Kosice, Jesenna 5, 041 54 Kosice, Slovakia
[c] Institute of Animal Biochemistry and Genetics, Centre of Biosciences, Slovak Academy of Sciences, Dubravska cesta 9, 840 05 Bratislava, Slovakia

ARTICLE INFO

*Keywords:*
Low-density lipoprotein
High-density lipoprotein
Hypericin
Transport
Cancer
Photodynamic therapy
CAM model

ABSTRACT

Lipoproteins are very attractive natural-based transport systems suitable for applications in diagnostics and cancer therapy. Low- and high-density lipoproteins (LDL, HDL) were selected for hypericin (hyp) delivery in cancer cells. Hyp was used, as it is a well-known model for hydrophobic molecules, in order to estimate the LDL and HDL transport efficacy. We applied fluorescence techniques, absorption and Raman spectroscopy to characterize the state and alteration of LDL and HDL in the absence and presence of hyp. The fluorescence intensity of hyp loaded in lipoproteins was two times weaker in HDL than LDL. We demonstrated that there are faster redistribution kinetics of hyp from HDL than from LDL. As a consequence, hyp uptake by glioma and breast cancer cells was driven more *via* endocytosis when hyp was delivered by LDL than by HDL. Hyp induced photodynamic action was stronger when hyp was delivered by HDL than LDL. *Ex ovo* hyp fluorescence pharmacokinetics demonstrated differences in biodistributions of hyp in lipoproteins topical applications. However, hyp was successfully delivered to cancer cells grafted on quail's chorioallantoic membrane. The results presented in this paper could provide strategies to develop adequate and targeted anticancer therapy.

## 1. Introduction

Non-specific accumulation of anticancer drugs in cancer tissue gave rise to many efforts from researchers to develop a transport system which would meet certain specific targeting requirements. Excellent transport systems would improve the selectivity of a chemotherapeutic agent, the hydrophobic drug stability, and its solubility in order to prolong and control the drug release, therefore lowering its cytotoxicity to healthy tissue. The field of nanosystems and nanoparticles, derived from the field of nanotechnology, is currently a highly studied research field. Besides development of a nanodelivery system based on liposomes, micelles, nanotubes or polymeric conjugates, endogenous lipoproteins still represent very interesting natural carriers suitable for drug delivery, as well as for tumor-targeted therapies [1–3].

Primarily, targeting is very important in the delivery of a photosensitizer (PS). PS is characterized by photodynamic properties that virtually combine tumor diagnostics and treatment modalities in one step [4]. PS can often be highly specific and localized in tumor tissue. Thanks to PS fluorescence, surgeons can easily identify damaged tissue. Photodynamic therapy (PDT) employs PS, oxygen, and light at specific wavelength that coincide with the absorption properties of PS, thus enabeling the excited PS triplet state to interact with oxygen [5,6]. Generation of highly reactive oxygen species (ROS) are often the result of such interaction. Specific localization of PS together with the high reactivity of ROS with cancer cells should ensure minimal invasiveness of PDT. Moreover, the nearby healthy tissue, in its ideal condition, would persist unharmed.

Hypericin (hyp) was identified many times as a suitable PS for photo-diagnostics and photo-treatment [7–10]. Hyp is a hydrophobic molecule characterized by a broad absorption spectrum in the visible region and emission above 600 nm [7]. It can be excited with blue/green light in photo-diagnostics, and with orange/red light in photo-treatment. It was demonstrated that PDT induced by hyp might trigger apoptotic signaling pathways in cancer cells [8,11–13]. Our experiment, which is strongly supported by literature, allows us, in many aspects, to considered hyp as an appropriate model molecule of

* Corresponding author.
*E-mail addresses:* lenka.lenkavska@gmail.com (L. Lenkavska), ludmila.blascakova@upjs.sk (L. Blascakova), zuzana.jurasekova@upjs.sk (Z. Jurasekova), Mariana.Macajova@savba.sk (M. Macajova), Boris.Bilcik@savba.sk (B. Bilcik), cavarga.ivan@gmail.com (I. Cavarga), pavol.miskovsky@upjs.sk (P. Miskovsky), veronika.huntosova@upjs.sk (V. Huntosova).

https://doi.org/10.1016/j.pdpdt.2018.12.013
Received 9 October 2018; Received in revised form 12 December 2018; Accepted 27 December 2018
Available online 28 December 2018
1572-1000/ © 2018 Elsevier B.V. All rights reserved.

hydrophobic PS and anticancer drug.

Intravenous administration of hydrophobic drugs is problematic. For this reason, they need to be embedded in a biocompatible transport system. Lipid-based formulation of nanoparticles, to a large extent, fits the above-mentioned requirements [14–16]. The most interesting natural lipid-based transport systems are endogenous lipoproteins. Low-density lipoprotein (LDL) is a globular particle, with a diameter around 22 nm, which is made up of a hydrophobic core and amphipathic phospholipids shell with a single apo B-100 protein [17]. LDL molecules are transported into cells *via* LDL receptors mediated endocytosis [18,19]. It was reported that most of the cancer cells expressed elevated numbers of LDL receptors to supply cells with cholesterol, which is endogenously transported by LDL in the bloodstream [20,21]. These properties identify LDL as one of the best components in the concept of an effective transport system for hydrophobic drugs in cancer targeted therapies.

When compared to LDL, high-density lipoproteins (HDL) represent smaller particles (~ 10 nm in diameter). In contrast to LDL, it is composed by apo A and apo C proteins [22]. HDL is, similarly to LDL, responsible for cholesterol transport to and from the tissues. It was found that drugs incorporated in HDL were more cytotoxic to cancer cells than if they were applied solely [23]. However, HDL uptake by cells differs from that of the LDL [24]. HDL can only be internalized *via* certain type of endocytosis, while LDL are degraded in lysosomes. Indeed, the catabolism of HDL in cells is still unknown.

Application of LDL and HDL as a PS carrier in PDT of cancer cells is not a completely new idea. It was already demonstrated that LDL could effectively deliver PSs (porphyrins, chlorines, berberine and hypericin) to cancer cells [25–32]. Thanks to the high LDL receptors affinity, LDL could increase PDT specificity in certain types of tumors [33,34]. Unfortunately, pathogenic events, such as chemical and oxidative stress, ageing, and other stimuli modify the LDL structure, which considerably influences its uptake by cells [35]. It was also demonstrated that the hydrophobicity of PS importantly influences its affinity to both LDL and HDL [32]. Moreover, PS accumulation in different blood components can be controlled by the rational design of PS [31]. Therefore, modification of LDL or HDL could enhance the targeting and efficiency of PDT [36,37].

Chorioallantoic membrane (CAM) of chicken or quail embryos is a very attractive model of microcirculatory system that can be used for PS pharmacokinetics and tumor targeting studies [38–42]. We demonstrated previously that hyp and hyp bound to LDL can be topically or intravenously applied to CAM [41–43]. Moreover, thanks to its fluorescence, it can be directly detected in the CAM bloodstream or xenografted cancer cells [41,43].

In the present study, our aim is to compare LDL and HDL, and investigate its impact on PS (hyp) delivery, the PDT efficacy, and to visualize hyp tumor targeting in the CAM model.

## 2. Material and methods

### 2.1. Cell culture

The U87 MG (human glioma) cells were purchased from Cells Lines Services, Germany. BT 474 (human breast ductal carcinoma) and SK BR 3 (human breast adenocarcinoma) cells were a gift from prof. Pluckthun's laboratory, University of Zurich, Switzerland. Cells were grown in the dark at 37 °C, 5% $CO_2$ and humidified atmosphere until 80% confluence. U87 MG cells were grown in culture medium (Dulbecco's modified Eagle medium, D-MEM) supplemented with 10% fetal bovine serum (FBS), L-glutamine (862 mg/l), sodium pyruvate (110 mg/l), glucose (4500 mg/l) and penicillin/streptomycin (1% w/w). For BT 474 and SK BR 3 cells, D-MEM was replaced by RPMI 1640 (LM-R1638/500, biosera), containing 25 mM Hepes, stable glutamine. All solution for cell culture were purchased from Gibco-Invitrogen, Life Technologies Ltd.. One day before the experiment, the 10% FBS was replaced by 2% Ultroser™ G serum (Pall, France), a serum substitute (2% UG), in order to maintained the cells in a lipids free cell culture medium.

### 2.2. Absorption and fluorescence spectroscopy

The stock solution of 2 mM hypericin (hyp, Sigma-Aldrich, Slovakia) was prepared by dissolving hyp in 100% dimethylsulfoxide (DMSO, Sigma-Aldrich, Slovakia). The hyp solution aliquots were mixed with LDL and HDL in order to form complexes with defined concentration ratios in a phosphate saline buffer at pH = 7.4 (PBS, Sigma-Aldrich, Germany). LDL (human low-density lipoproteins, purity > 98% of total lipoprotein content by electrophoresis, Calbiochem, Germany) and HDL (human high-density lipoproteins, purity > 95% of total lipoprotein content by SDS-PAGE, Sigma-Aldrich, USA) stock solutions were first diluted in PBS, then mixed with a solution of hyp. DMSO content in the prepared complexes was less than 1%. The complexes of hyp with LDL (hyp:LDL) and HDL (hyp:HDL) were stabilized overnight in the dark at 4 °C. LDL and HDL concentrations in complexes were fixed at 10 nM.

LDL and HDL UV–Vis absorption spectra were detected with Specord 600 diode-array spectrometer (Analytik Jena AG, Germany) at room temperature. Absorption was collected every 0.5 nm in the spectral range 260–750 nm.

The fluorescence spectra of hyp:LDL and hyp:HDL complexes (3:1, 10:1, 30:1, 50:1 and 100:1) were detected with a spectrophotometer (RF-5301 PC, SHIMADZU, Japan) at 560 nm excitation. The detection window was between 580–750 nm (5 nm and 10 nm slits), and the maximum of the fluorescence intensity was estimated at 600 nm. The obtained spectra and data were processed with the Origin9 software (OriginLab®, Massachusetts, USA).

### 2.3. Surface-enhanced Raman spectroscopy (SERS)

SERS measurements were carried out using a Raman inVia microspectrometer (Renishaw, Great Britain) equipped with an electrically cooled CCD camera, working under macro conditions using glass vials and excitation wavelength at 532 nm. The laser power used on the sample did not exceed 50% of its original power. SERS spectra were recorded on the silver colloid prepared by chemical reduction of silver nitrate with hydroxylamine hydrochloride (AgH) [44]. The aqueous solutions utilized for the colloidal nanoparticles formation were prepared by using milli-Q water, and all the employed reagents were purchased from Sigma-Aldrich (Slovakia). The resulting AgH colloid showed a gray-brown color with a plasmon extinction band at 405 nm and final pH of 5.5. The colloid was activated before the addition of an aliquot of the LDL/HDL solution, in order to achieve a much larger SERS effect [45]. The 10 μM stock solutions of LDL and HDL were used and the final concentration of LDL/HDL in SERS experiments was 5 nM. The same final concentration of lipoproteins was adjusted for hyp:LDL and hyp:HDL complexes (10:1, 50:1).

### 2.4. Western blot

The oxidative phosphorylation OXPHOS profile and LDL receptors expression of U87 MG cells were estimated by western blot. The OXPHOS optimized antibody cocktail (1:500, ab110411, Total OXPHOS Human WB Antibody Cocktail, abcam, UK) contained 5 antibodies against CI-NDUFB8 (NADH dehydrogenase (ubiquinone) 1 beta subcomplex subunit 8, ab110242), CII-SDHB (succinate dehydrogenase subunit B, ab14714), CIII-UQCRC2 (ubiquinol-cytochrome c reductase core protein 2, ab14745), CIV – COXII (cytochrome c oxidase subunit 2, ab110258) and CV-ATP5A (ATP synthase subunit alpha, ab14748). LDL receptor expression was evaluated by anti-LDL receptor antibody (1:1000, ab30532, anti-LDL receptor antibody, abcam, UK). The analysis was performed on U87 MG cells subjected for 1 h to 50 nM LDL and HDL. Briefly, cells were harvested, lysed in a RIPA buffer (150 mM

NaCl, 1% Triton X-100, 0.5% sodium deoxycholate, 0.1% sodium dodecyl sulfate, 20 mM Tris buffer saline at pH 8.0) with an inhibitor cocktail (2 × 1:100, Halt™ Protease & Phosphatase Inhibitor Cocktail, ThermoFisher Scientific, USA). Whole lysate (120 µg of total protein amount) were diluted in 2x Laemmli buffer (Sigma-Aldrich, Germany) to reach 60 µg of final protein amount, loaded to 10% (OXPHOS) and 8% (LDL receptors) polyacrylamide gel and subjected electrophoresis. Proteins were transferred to a nitrocellulose membrane. Immunodetection was performed with Western Breeze Chromogenic Kit (ThermoFisher Scientific, USA). Primary antibodies OXPHOS cocktail, LDL receptors and β-actin (1:2500, A5316-100UL, monoclonal Anti-β-actin antibody produced in mouse, Sigma-Aldrich, Germany) were incubated overnight with the membrane at 4 °C. Secondary antibodies Western Breeze Chromogenic Kit for detection of rabbit and mouse primary antibodies were used to visualize LDL receptors and β-actin, OXPHOS, respectively. Densities of visualized bands were calculated with ImageJ software (National Institutes of Health, USA).

### 2.5. Stopped-flow

For the hyp redistribution kinetics measurements, hyp:LDL and hyp:HDL complexes (50:1) were initially prepared at given concentration ratios. These complexes were stabilized overnight in dark conditions at 4 °C. Redistribution kinetics of 1 µM hyp from 10 nM LDL and HDL towards 10 nM free LDL were measured by a stopped-flow apparatus (Applied Photophysics, UK), according to the SX20 User Manual. A 150 W xenon lamp emitting light at 560 nm was used to excite the complexes, and hyp fluorescence was detected using long passed filter > 600 nm. Detection time range was 5 s, 40 s, 200 s and 1000 s.

Analysis and kinetics were processed with the Origin9 software. Mono-exponential fit $y = y_0 + Ae^{(-x/t)}$ was applied to all obtained curves. Parameters of the fit are summarized in the table.

### 2.6. Confocal fluorescence microscopy

Cells were grown in glass coverslip bottom Petri dishes (35 mm, No. 0, MatTek, USA) at a density of $10^4$ cells. 10 nM concentration of LDL and acetylated LDL labeled by Dil ($LDL_{Dil}$, $acLDL_{Dil}$, ThermoFisher SCIENTIFIC, Germany) were applied to study the endocytotic pathway in U87 MG cells. 50 nM concentration of LDL and HDL loaded with 500 nM hypericin were applied to study hyp distribution and its uptake by U87 MG, SK BR 3 and BT 474 cells. Fluorescence images of hyp and Dil were collected from live cells 1 h after incubation with $LDL_{Dil}$, $acLDL_{Dil,}$ and hyp in complexes with LDLs or HDL at hyp:LDL and hyp:HDL ratio 10:1. An inverted LSM700 confocal microscope (Zeiss, Germany) was equipped with a 63X oil immersion objective (NA = 1.46, with adjustable coverslip correction) and a CCD camera (AxioCam HRm, Zeiss, Germany). Hyp and Dil were excited with a 555 nm cw solid-state laser, and the emission was detected at > 590 nm. The fluorescence images were analyzed with Zen 2011 software (Zeiss, Germany) or ImageJ software (National Institutes of Health, USA). A cell culture medium for microscopic observation contained phenol red, but it did not affect the fluorescence detections.

### 2.7. MTT-assay

U87 MG cells were subjected to photodynamic treatment 24 h before MTT-assay. Cells were subjected for 1 h to 500 nM hyp, 500 nM hyp in 50 nM LDL and 500 nM hyp in 50 nM HDL. After incubation, the cell culture media were replaced by fresh medium (without hyp, HDL, and LDL) and incubated in the dark or irradiated on home-made irradiation diode platform at 590 nm and fluence 4 J/cm$^2$. Cell response was validated 24 h after these treatments.

U87 MG, SK BR 3 and BT 474 cells were subjected to photodynamic treatment 5 h before the MTT-assay. Cells were subjected for 1 h to 500 nM hyp in complex with 10 nM LDL (50:1). After incubation, the cell culture media were replaced by fresh medium (without hyp and LDL) and incubated in the dark or irradiated on home-made irradiation diode platform at 590 nm and fluence 4 J/cm$^2$. The values obtained for U87 MG control cells were adjusted as a 100% proliferation, and compared with the other cell lines and treatments. Difference between control and PDT subjected cells was determined to evaluate the efficacy of the treatment.

Cell viability was assessed by MTT (3-(4,5-dimethylthiazol-2-yl)-2,5-diphenyltetrazolium bromide, Sigma-Aldrich, Germany) assay detected at 560 nm and 750 nm by 96 well plate absorption reader (GloMax®-Multi + Detection System with Instinct Software, Promega Corporation, USA). A standard protocol for MTT-assay was performed: 10 µl of 5 mg/ml MTT dissolved in phosphate saline buffer (PBS, pH = 7.4) was added to each well filled with 100 µl medium, and the plate was incubated for 2 h in the dark at 37 °C; after 2 h, the 50 µl of cell culture medium were removed from the well and 150 µl of acidic iso-propanol (Sigma-Aldrich, Germany) was added to each well to dissolved formazan crystals.

The errors are represented by SD or SEM from the mean values of the experimental data (performed in triplicates). The level of significance was estimated with T-test: *$p < 0.05$, **$p < 0.01$, ***$p < 0.001$.

### 2.8. Quail chorioallantoic membrane ex ovo model with grafted cancer cells

Fertilized Japanese quail (*Coturnix japonica*) eggs (breeding colony of IABG SASci) were incubated in a forced draught incubator (MIDI BIOS, Czech Republic) at 37 °C and 50–60% relative humidity. To prepare *ex ovo* culture, the surface of the eggs was disinfected with 70% ethanolic solution at embryonic day 3 (ED3) in a sterile laminar flow hood. The eggs were opened, and the embryos were transferred into six-well tissue culture plates (Sarstedt, Germany) and returned to a 37 °C humidified incubator (Memmert, Germany).

On ED7, the silicone ring (⌀ 6 mm) was positioned on the CAM surface. The SK BR 3 and BT 474 cells (8 × $10^5$ cells per embryo in 30 µl RPMI solution) were implanted in the ring.

### 2.9. Topical pharmacokinetics of hyp in the presence of LDL and HDL

On ED10, 72 h after cells implantation, hyp, hyp:LDL (20:1), hyp:HDL (20:1) were topically applied on CAM (hyp dose was 2 µg/g of the embryo, which is 79 µM in PBS, the DMSO content was 0.17%). Fluorescence intensity of hyp in CAM tissue and cancer cells was recorded using a digital camera (Canon EOS 6D II with Canon MP-E 65 mm f/2.8, Japan) at 0, 1, 3, 5 and 24 h after substance administration. The CAMs were illuminated using either white light (ring flash Canon MR-14EX, Japan), or by violet excitation light (custom made circular blue LED light emitted at 405 nm). The fluorescence intensity was evaluated using ImageJ software [46]. RGB image channels were split into separate red, green and blue images. Red intensity images were analyzed in 8-bit forms. Red intensity was evaluated from the whole image and approximated as the hyp fluorescence. Whole images profile plots (ImageJ plugin) were derived for each time after hyp administration: from 0 (right after administration) up to 24 h.

### 2.10. CAM histology

On ED11, CAM tissue was separated and fixed with 4% paraformaldehyde (Sigma-Aldrich, Germany). Subsequently, 4 µm paraffin sections were prepared for histopathological analysis to determine malignancy and surrounding healthy tissue (hematoxylin, BAMED, Slovakia and eosin, BAMED, Slovakia, staining). Stained sections were evaluated using a light microscope Kapa 2000 (Kvant, Slovakia) with 10X and 20X objective and Nikon E995 digital camera (Japan).

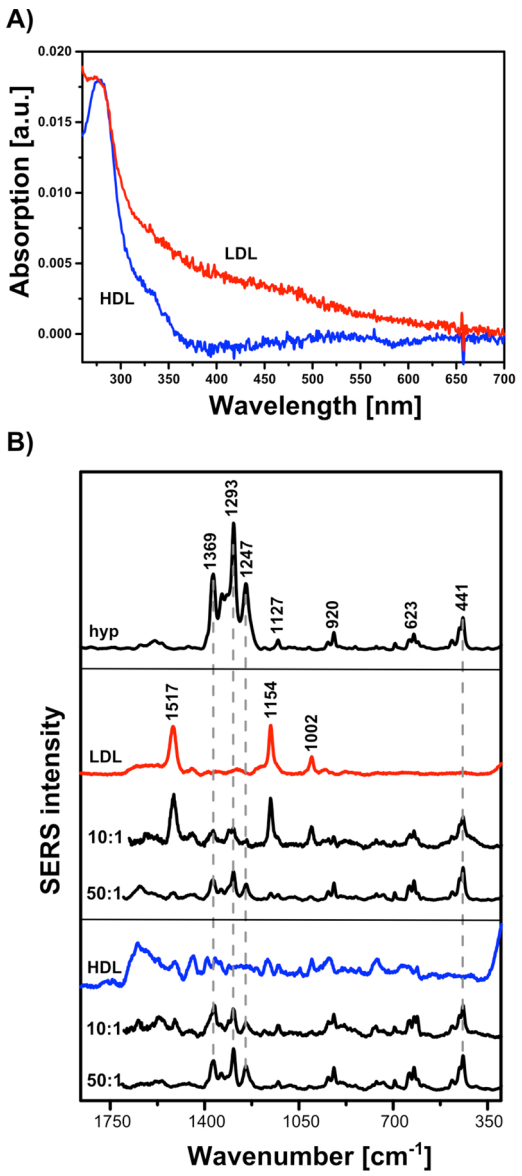


**Fig. 1.** A) UV-Vis absorption spectra of LDL (red) and HDL (blue) in PBS solutions at pH = 7.4. B) SERS spectrum of hyp, low-density lipoproteins (LDL, red) and high-density lipoproteins (HDL, blue) in the absence and in the presence of hyp at concentration ratios 10:1 and 50:1 (hyp:LDL or hyp:HDL). The final concentrations of LDL and HDL were 5 nM. The excitation line is at 532 nm. All spectra were corrected by baseline subtraction.

## 3. Results and discussion

### 3.1. Characterization of LDL and HDL by optical spectroscopy methods

Spectroscopic methods can divulge important information not only about the physico-chemical characteristics of the PS and host molecules, but also about the mechanism of their interactions. In particular, the knowledge of structural and vibrational spectroscopic properties of lipoproteins is highly desirable, since their alteration can significantly affect their behavior and functioning as a transport system. Accordingly, the loading capacity as a parameter of different lipoproteins' composition can also be investigated spectroscopically by use of hyp as a model of hydrophobic PS.

#### 3.1.1. UV–Vis absorption spectra

UV-Vis absorption spectra of 10 nM LDL and HDL solutions are presented in Fig. 1A. Both lipoproteins are principally characterized by the main absorption band at 280 nm, which corresponds with their protein content. However, in the case of LDL solution, a broad lipids-assigned band found in the range of 300–650 nm can also be demonstrated. The presented spectra have been previously observed [61,72]. However, LDL and HDL extracted from human plasma are not uniform, and their composition can be particularly affected by other components (such as fatty acids, *etc.*). Thus, it is always recommended, even necessary, to detect and characterize them quickly. After that, more detailed information about the PS and LDL or HDL structure, even at such low concentrations, can be obtained from their SERS spectra.

#### 3.1.2. SERS spectra

Raman spectroscopy (RS), because of its non-destructiveness and high chemical specificity, seems to be an appropriate method for quick and unambiguous identification of LDL and HDL state [47,48]. Furthermore, SERS reflects the same specific structural and chemical information as RS, but provides additional advantages such as increased intensity of normally weak Raman signal and quenching of usually strong fluorescence background [49].

Fig. 1B shows the SERS spectra of 5 nM LDL and HDL solutions recorded on the AgH colloid while using a 532 nm laser excitation. Despite a very low concentration of lipoproteins, intense and well-defined Raman bands, visible especially in the SERS spectrum of the LDL solution (Fig. 1B **'LDL'**), were recorded as a result of the employment of metal nanoparticles and pre-resonance excitation wavelength. The SERS spectrum of LDL is characterized by relatively strong and sharp Raman bands at 1517, 1154 and 1002 $cm^{-1}$, which correspond to carotenoid compounds naturally present in LDL structure, in particular all-*trans*-*β*-carotene and lycopene [48,50]. Taking into account only slight spectral changes observed in the SERS spectrum of LDL (Fig. 1B **'LDL'**) with respect to the classical Raman spectrum of the β-carotene [51,52], we assume that β-carotene after the adsorption of LDL particles upon the silver surface remains incorporated in the LDL, which are located rather close to the surface than deep in the core of the LDL. Lin S. et al. demonstrated that the carotenoids are accessible close to the surface of the LDL particles in the shell, where apo B-100 is located [50]. The rest of the bands associated with the major components of the lipoproteins (apolipoprotein, cholesteryl ester, triacylglycerol and phospholipid) do not contribute significantly to the recorded SERS spectrum. The situation changes in the case of HDL, where β-carotene is commonly present only in small portions; thus, no intense and well-defined spectral features are visible. The SERS spectrum of HDL (Fig. 1B **'HDL'**) shows a series of bands associated mainly with lipids and proteins, whose positions and corresponding vibrational assignments are discussed in greater detail elsewhere [53].

In order to study hyp:lipoprotein complexes and to monitor variances between them, the SERS spectra of hyp:LDL and hyp:HDL at two different ratios, 10:1 and 50:1, were also recorded (Fig. 1B**, '10:1'and '50:1').** While the SERS spectrum of hyp:LDL at the 10:1 ratio exhibits a mixture of bands due to both LDL and hyp, the SERS spectrum of hyp:LDL at higher ratio is practically dominated by the intense Raman bands of Hyp (Fig. 1B**, '10:1'and '50:1'*top*, 'hyp'**). It has already been shown [54] that at the low ratio, the PS molecule is located in the inner part of the LDL particle. However, when the concentration of hyp increases, the progressive localization of hyp molecules in the outer shell of LDL takes place. Moreover, the SERS bands at 1247, 1293, and 1369 $cm^{-1}$, clearly visible in the SERS spectrum of hyp:LDL at the 50:1 ratio, are characteristic of hyp monoanionic form. The amphipathic outer part of the LDL particle containing phospholipids and apo B-100 protein is a favorable environment, where interaction of hyp with the polar groups of these biomolecules can likely occur.

The SERS spectra of hyp:HDL complexes measured for both ratios (Fig. 1B**, '10:1'and '50:1'*below*)** show great similarities, as the obtained spectra are mostly determined by the hyp spectral features. In accordance with the LDL-complexes, the SERS spectrum of hyp:HDL at

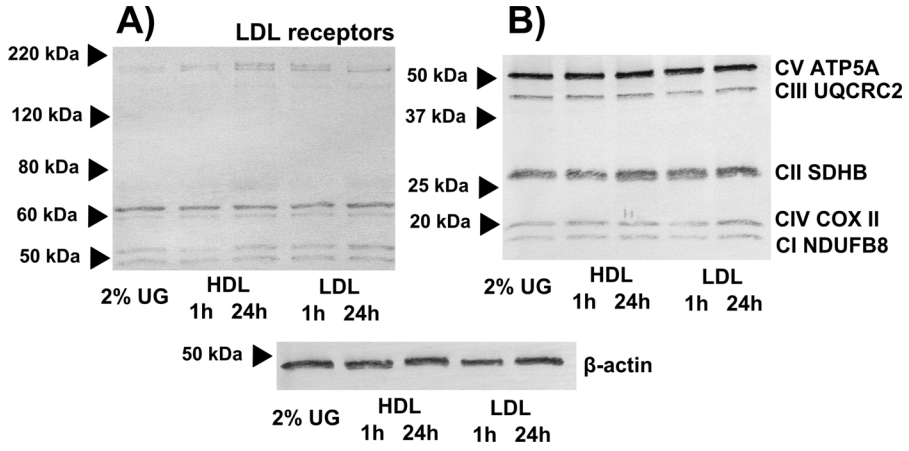


**Fig. 2.** Expression of A) LDL receptors and B) CI-CV complexes of respiratory chain in U87 MG after 1 h and 24-hour subjection to 50 nM LDL and HDL in the absence of lipids in cell culture media (2% UG) analyzed by western blot. β-actin was used as a loading control.

the 10:1 ratio still possesses some of the bands characteristic of the lipoprotein. However, the intensity of hyp Raman bands is significantly higher. This enhancement is even more pronounced at higher ratio (50:1), which is probably due to the same effects as in the case of LDL: increase of hyp concentration followed by the progressive localization of hyp in the outer shell of LDL. The HDL is smaller and contains a higher protein content than the LDL particle. Thus, the PS molecule bind more easily to the lipoprotein surface, which could also significantly affect its release speed.

### *3.2. Characterization of LDL receptors and oxidative stress in cancer cells subjected to LDL and HDL*

It is generally assumed that cancer cells express a higher number of LDL receptors to ensure cholesterol supply for membrane construction [19–21]. However, not all cancer cells express exactly the same number of LDL receptors [33,34]. It was previously reported that glioma cells are a type of tumor with an elevated expression of LDL receptors [33,55]. Fig. 2A demonstrates a western blot analysis of U87 MG cells LDL receptors and related proteins. Several bands were detected in the range between 50 and 220 kDa in control and lipoproteins (LDL/HDL) subjected cells. Higher density bands (below 220 kDa molecular weight) were observed in cells subjected to 50 nM LDL (1 h and 24 h) and HDL (24 h), compared to the non-treated control. Our results suggest that LDL presence in lipid-starved cell culture media increased LDL receptor expression in U87 MG cells. However, HDL has to be incubated for 24 h with U87 MG cells in order to reach a similar effect, which can be achieved with LDL in a shorter period of time (1 h). Keep in mind that this delay could be explained by the composition of LDL and HDL, which undergo different type of endocytosis and catabolism in the cells [24].

Although lysosomes are the predominant targets of LDL receptor-mediated endocytotic pathway [18,19], cell apoptosis can be triggered by oxidative stress produced in mitochondria [4,56]. Fig. 2B presents a western blot analysis of the respiratory chain complexes expressed in U87 MG cells, in the presence and absence of LDL and HDL. We did not find any significant changes of western blot band densities in the cells subjected for 1 h or 24 h to the studied lipoproteins. This observation suggests that cells could overcome some level of oxidative stress, even if it was possibly triggered by long-term incubation with LDL and HDL.

### *3.3. Redistribution of hypericin from LDL and HDL towards free LDL*

Hyp, in this study, represents a model of a hydrophobic molecule with promising anticancer properties, especially in photodynamic treatment [7,8]. It was demonstrated that only hyp monomers emit fluorescence [57–59]. Other researcher groups, along with ours, observed that a high number of hyp molecules could be loaded in LDL, but this process is accompanied by aggregation and self-quenching of hyp molecules inside LDL [57,59–61]. We noticed that the ratio between hyp and LDL at which hyp started its aggregation process varied from case to case. It should be noted that lipoproteins are extracted from human serum, and the precise protein and cholesterol content may differ as well. For this reason, we performed experiments in order to estimate the aggregation and fluorescence intensity plateau of hyp in LDL and HDL. We observed that, in LDL, the hyp:LDL ratio is 50:1, while in HDL it is 10:1 (Fig. 3A). The hyp intensity is four times weaker in HDL than in LDL at the ratio 50:1. In the latest study, we demonstrated that hyp aggregation process can play an important role in the redistribution of hydrophobic molecules from transported LDL particles towards free CAM serum components in bloodstream [43].

Fast hyp redistribution kinetics from LDL and HDL towards free LDLs were detected by stopped-flow technique. In respect to the results demonstrated in Fig. 3A, we used hyp:LDL and hyp:HDL concentration at ratio 50:1. The redistribution processes were observed in a time scale of 5 s, 40 s, 200 s and 1000 s (Fig. 3B). We did not observe differences between the two studied cases in very fast processes within 5 s. The sharp increase in redistributive function was detected for hyp redistribution from HDL between 40 and 200 s. The evident exponential character of these functions was recorded at a time scale of 1000 s. Much slower hyp redistributions were noticed for hyp redistribution from LDL. Hyp redistribution gently increased at 200 s, but remarkable progress was recognized at 1000 s scale in Fig. 3B. In contrast, hyp redistribution from HDL showed a steep beginning that reaches its maximum at 400 s. The fitting parameters of redistributive processes are summarized in Table 1.

We observed mono-exponential processes in our studied conditions. The precision of mono-exponential fits was the best at 200 s and 1000 s kinetics ($R^2$ close to 1). Halftime (t) of hyp redistribution was shorter for HDL (200 s and 188 s, respectively) and larger for LDL (529 s and 796 s, respectively). This halftime was, in our previous studies, defined as the slow component of hyp redistributive process [37,57]. The slow component was much faster in hyp redistribution from HDL. This suggest that the incorporation of hyp in LDL and HDL is not the same, and that the hyp affinity to HDL could be weaker. The rate of hyp redistribution from LDL/HDL could reflect the hyp ability to pass through the plasma membrane of cancer cells. We assumed that hyp uptake by cells would be better when HDL delivers hyp than LDL. While with HDL transport, the cellular uptake may compose of both diffusion and endocytosis, with LDL the majority of transport processes are governed *via* endocytosis. An even more critical point is that these processes can occur during the hyp delivery by LDL and HDL *in vivo*.

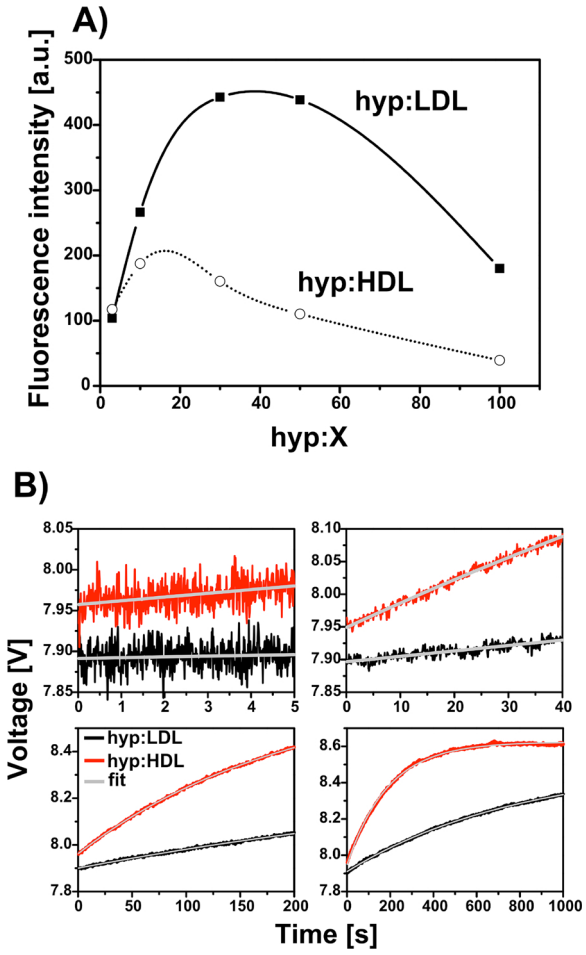


**Fig. 3.** A) Fluorescence intensity of hyp in the presence of 10 nM LDL (black squares, solid line) and HDL (open circles, short dot line) in PBS at pH = 7.4. Hyp concentration increases as indicated with the concentration ratios hyp:X, where X represents LDL and HDL. B) Representative kinetics of hyp redistribution from LDL (black lines) and HDL (red lines) towards LDL detected by stopped flow technique. Detection times are at x-axes: 5 s, 40 s, 200 s and 1000 s. Kinetics were fitted (gray lines) with mono-exponential fits and their parameters are summarized in Table 1.

**Table 1**
Parameters of redistribution kinetics (Fig. 4) determined with mono-exponential fit: $y = y_0 + Ae^{(-x/t)}$.

| time range | 100:1 | $y_0$ | A | t [s] | $R^2$ |
|---|---|---|---|---|---|
| 1000 s | hyp:LDL | 8.5 | -0.59 | 796 | 0.99 |
| | hyp:HDL | 8.6 | -0.68 | 188 | 0.99 |
| 200 s | hyp:LDL | 8.4 | -0.47 | 529 | 0.99 |
| | hyp:HDL | 8.7 | -0.72 | 200 | 0.99 |
| 30 s | hyp:LDL | 10.4 | -2.48 | 2959 | 0.73 |
| | hyp:HDL | 8.7 | -0.77 | 199 | 0.98 |
| 5 s | hyp:LDL | 7.9 | -0.03 | 27 | 0.01 |
| | hyp:HDL | 8.8 | -0.88 | 191 | 0.16 |

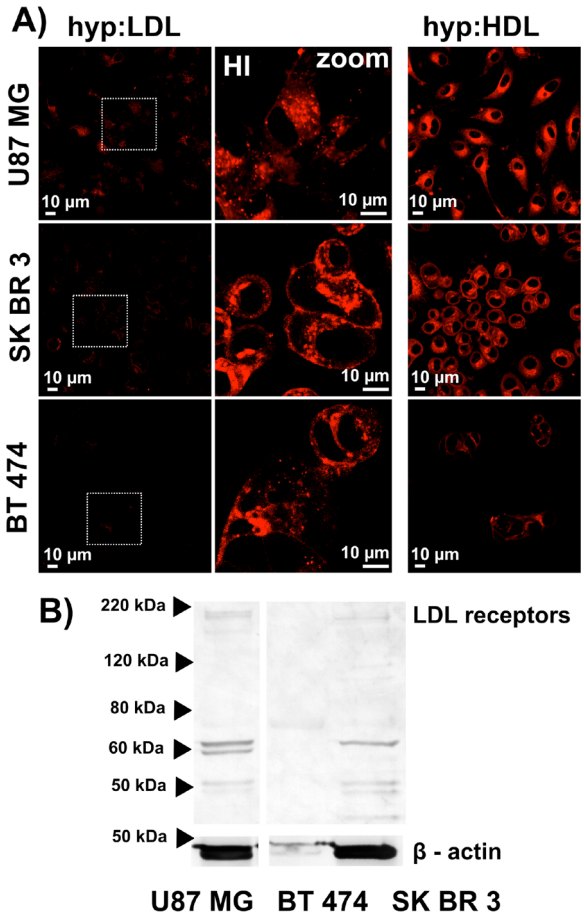


**Fig. 4.** A) Representative confocal fluorescence images of hyp distribution in U87 MG, SK BR 3, BT 474 after delivery by LDL (hyp:LDL) and HDL (hyp:HDL). HI represents zoomed image with higher fluorescence intensity. B) Western blot analysis of LDL receptors in U87 MG, BT 474 and SK BR 3 cells (at the same protein content). β-actin was used as a loading control.

### *3.4. Hypericin distribution and uptake by cancer cells after hypericin delivery in LDL and HDL*

Distribution and uptake of hyp in LDL and HDL by U87 MG, SK BR 3 and BT 474 cells is demonstrated in Fig. 4A. Hyp transported by LDL, which persists together with LDL and its intracellular distribution, was visible in the punctuated-lysosomal pattern. On the other hand, hyp was released faster from HDL, and diffused homogenously into cancer cells. The intracellular intensity of hyp fluorescence was higher when delivered by HDL than LDL. Moreover, the uptakes of hyp transported in both LDL/HDL by U87 MG cells were higher than the hyp uptakes by SK BR 3, and it was even higher than hyp uptakes by BT 474 cells. These behaviors were reflected by a decrease in fluorescence intensities in Fig. 4A.

If we consider that hyp:LDL complexes would pass the plasma membrane of cancer cells *via* LDL-mediated endocytosis, the lowest concentration (fluorescence intensity) of hyp would be in cells with a very low expression of LDL receptors. Western blot analysis of LDL receptors expression in U87 MG, SK BR 3 and BT 474 cancer cells is depicted in Fig. 4B. BT 474 cells expressed the fewest LDL receptors, while U87 MG cells have the highest level among all three studied cancer cell lines. Regarding the statement mentioned above, hyp:LDL complexes uptakes (*via* LDL receptor-mediated endocytosis) results are in accordance with LDL receptor expression observed by western blot analysis in these three cell lines.

Next, we monitored the hyp distribution and uptake in complexes with acetylated LDL, in order to better understand the high and

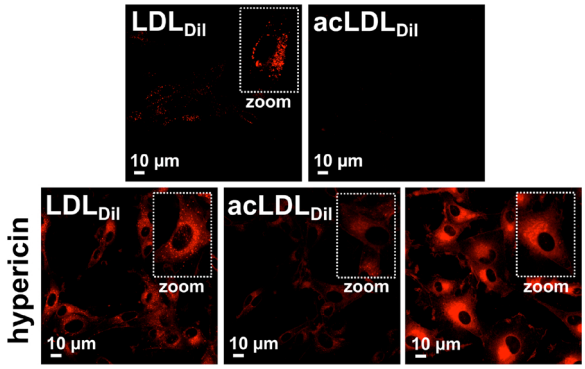


**Fig. 5.** Representative confocal fluorescence images of DiI labeled LDL (LDL$_{DiI}$) and acetylated LDL (acLDL$_{DiI}$) in U87 MG cells (first row). The second row represents the hyp distribution in U87 MG cells after hyp delivery by LDL$_{DiI}$, acLDL$_{DiI}$, and in the absence of LDL. Fluorescence intensity of zoomed insets is corrected to demonstrate hyp distribution in cell.

nonspecific distribution of hyp delivered by HDL in cancer cells (hyp:HDL in Fig. 4A). Both types of LDLs (acetylated and not-acetylated) were labeled with DiI, which emitted an orange fluorescence. One should pay attention in this case, as DiI fluorescence can be cross-correlated with hyp fluorescence. However, we assumed on the bases of our results that DiI would persist in LDL (localization in round spots), and that released hyp would be homogenously redistributed within the cell. We expected that acetylated LDL$_{DiI}$ (acLDL$_{DiI}$) would not be recognized by LDL receptors, therefore it should not pass through the plasma membrane of U87 MG cells.

It was reported that acLDL are not governed by LDL receptor-mediated endocytosis in cancer cells [62], possibly due to the acetylation of LDL that decreases the ability of LDL to interact with LDL receptors [62,63]. Albeit, it was shown elsewhere that fibroblasts and smooth muscle cells could increase their uptake of acLDL, because of the specific acetylated LDL receptors expression [64]. Fig. 5 demonstrates the localization of LDL$_{DiI}$ in lysosomes, but acLDL$_{DiI}$ fluorescence was not observed within U87 MG cells.

Further, we followed the hyp fluorescence and uptake by U87 MG cells in presence of LDL$_{DiI}$/acLDL$_{DiI}$. Previously, hyp could be recognized with the increasing of orange/red fluorescence, as well as a nonspecific but homogeneous distribution in cancer cells [9,30,55,65]. It was identified that strong hyp fluorescence in U87 MG cells corresponded to Golgi complex accumulation [9,30]. In Fig. 5, the highest fluorescence intensity was detected in cells subjected to hyp only. The weakest fluorescence intensity, as we expected, was detected in cells subjected to hyp transported by acLDL$_{DiI}$. More precisely, the numbers of fluorescent spots are visible in the zoomed area of LDL$_{DiI}$ fluorescence image (insets in Fig. 5).

On the other hand, nonspecific hyp localization was observed in cells subjected to hyp and hyp transported by acLDL$_{DiI}$. This suggests that hyp maintained in LDL$_{DiI,}$ was carried into the cells *via* endocytosis, similarly to hyp in LDL. Contrarily, hyp released from acLDL$_{DiI}$ diffuses in cells in a similar way as what is observed when HDL was used as the hyp transport system (Fig. 4A).

It should be noted that hyp fluorescence intensity was significantly weaker in acLDL$_{DiI}$ than LDL$_{DiI}$. Differences in cellular uptake for hyp:HDL and hyp:acLDL suggests two situations. Firstly, U87 MG cells can express some receptors for HDL uptake. Secondly, hyp affinity to LDL is so strong that hyp cannot be easily released from acLDL, as it is in the HDL case. We hypothesize that these receptors could also partially be LDL receptors related proteins, as we have demonstrated in Fig. 2A by western blot.

In general, specific intracellular distribution/localization of drugs can significantly influence the outcome of cancer therapy, especially PDT [66]. While mitochondrial localization of such molecules could result in apoptotic signaling pathways [67,68], lysosomal localization can result in their disruption and, in the end, the necrosis of the cell [69–71]. For this reason, an examination of therapeutically effective photosensitizer intracellular concentration and dosimetry is critical in PDT. Subsequently, the PDT efficacy induced by hyp after its LDL and HDL delivery was validated by MTT-assay.

### 3.5. The hypericin-induced photodynamic effect in cancer cells after hypericin delivery by LDL and HDL

Hyp was light activated in U87 MG cells subjected for 1 h to hyp, hyp in LDL and hyp in HDL. Using this short drug-light interval, we did not observe any significant inhibition of cell proliferation in the dark, as well as in cells subjected to hyp in LDL after irradiation with 4 J/cm$^2$ at

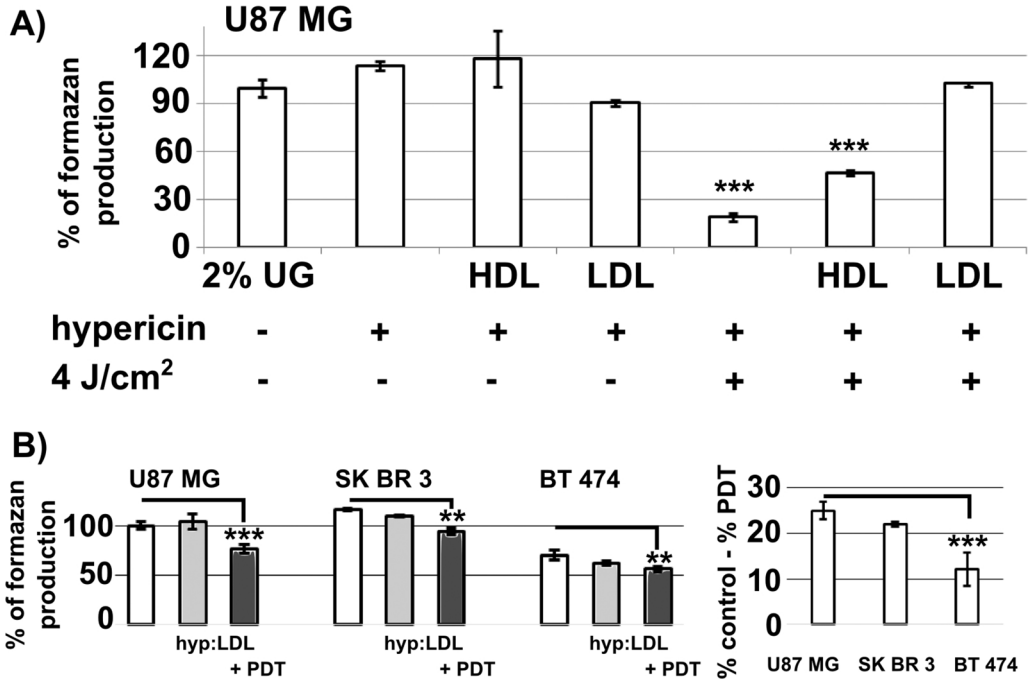


**Fig. 6.** A) MTT-assay of U87 MG cells subjected for 1 h to 500 nM hyp and hyp loaded in LDL and HDL (10:1), then kept 24 h in the dark or irradiated at 590 nm with fluence 4 J/cm$^2$. B) MTT-assay (performed 5 h after treatment) of U87 MG, SK BR 3 and BT 474 cells subjected for 1 h to 500 nM hyp loaded in LDL (50:1) and kept in the dark (light gray) without or with irradiation (+ PDT dark gray) at 590 nm with fluence 4 J/cm$^2$. Control cells are represented by the white columns. Mean value of U87 MG control cells was defined as 100% viable cells. Difference between % of cells without treatment (white columns) and % of cells after PDT (dark gray columns) is presented in right for each cell line. Error bars represent mean values from three independent measurements and significances were estimated with Student t-test, ***$p < 0.001$, **$p < 0.01$, *$p < 0.05$.

600 nm (Fig. 6A). However, a significant decrease in cell proliferation was detected in cells subjected to hyp alone and hyp in HDL after irradiation with 4 J/cm$^2$ at 600 nm. The considerable difference between photo-treatment induced by hyp and hyp delivered in LDL was denoted, and it is in agreement with previously reported results [30]. Hyp was located tightly inside the LDL particle at hyp:LDL concentration ratio 10:1 and passed into the cancer cells preferentially *via* endocytosis. We have reported that hyp at higher hyp:LDL concentration ratios (above 50:1) passed into the cells both *via* diffusion and endocytosis. We hypothesize that the endocytotic process is less effective to achieve sufficient hyp therapeutic concentration than passive diffusion in U87 MG cells.

We succeed in increasing the PDT efficacy when using HDL in comparison to LDL as the delivery system for hyp (Fig. 6A). Because of the results obtained by western blot, where HDL did not significantly influence LDL receptors and OXPHOS characteristics (Fig. 2A, B), enhancement of PDT efficacy can be explained by increasing the hyp concentration that can be photo-activated within U87 MG cells. Thus, low affinity of hyp to HDL enabled hyp release in higher concentration in cells (Fig. 4A). Moreover, endocytosis is not preferential pathway of hyp delivery in HDL in studied cancer cells. Thus, hyp diffusion into the cells from hyp:HDL will be more effective.

To ensure hyp:LDL targeted PDT, we validated the influence of LDL receptors expression in cancer cells to hyp induced PDT efficacy. In this study, hyp was delivered to U87 MG, SK BR 3 and BT 474 by LDL at hyp:LDL concentration ratio 50:1. We noticed a significant decrease in cells viability 5 h after hyp induced PDT (Fig. 6B). It should be noted that the proliferation of studied cancer cell lines in the absence of hyp was not the same. SK BR 3 cells proliferated more than BT 474 cells (50% of SK BR 3 proliferation rate). As we discovered previously, BT 474 cells expressed a low level of LDL receptors, which could significantly decrease the efficacy of hyp:LDL induced PDT. These results confirm that LDL receptors expression might considerably influence hyp induced PDT after delivery by LDL.

### *3.6. Hypericin topical pharmacokinetics and cancer cells delivery on quail CAM*

Topical pharmacokinetics of hyp is demonstrated in Fig. 7. We compared the fluorescence intensity of hyp in the absence (in PBS solution at pH 7.4) and presence of LDL and HDL topically applied on CAM with grafted SK BR 3 and BT 474 cells (Fig. 7A). The most intense hyp (pink) fluorescence was detected in complexes with LDL, and a very weak intensity was observed when hyp was administered in PBS solutions. Images plot profiles in Fig. 7B refer to 24-hour pharmacokinetics. The section delimited by the red arrow does not correspond to hyp, but white light image. For this reason, these intensities represent maximal and only informative detected values. Pharmacokinetics of hyp were similar in CAM with grafted SK BR 3 and BT 474 cells. SK BR 3 and BT 474 cells were applied as 30 µl droplets on the ectoderm of CAM. From the histological slices of normal CAM and CAM with grafted cancer cells, we observed that the applied cancer cells were maintained on the ectoderm and did not migrate to the mesoderm of CAM (data not shown). For this reason, we topically applied hyp, hyp:LDL and hyp:HDL solutions. Different distributions were observed after hyp administration in LDL, HDL, and PBS only (Fig. 7A, B). Hyp (applied in PBS) fluorescence increased with the time of incubation due to hyp monomers formation in CAM and cancer cells. Hyp:LDL fluorescence was detected for 5 h at the same level, and slightly decreased after 24 h. On the other hand, hyp:HDL fluorescence was, shortly after administration, weaker than hyp:LDL. At 1- and 3-hour post-administration, the hyp:HDL and hyp:LDL fluorescence intensities reached the same level. However, the hyp fluorescence intensity starts to decrease 5 h after the hyp:HDL administration. Due to the differences in hyp fluorescent pharmacokinetics, hyp fluorescence-based cancer cells detection could be performed at different period by the selection of appropriate transport system (HDL, LDL) and hyp:LDL/hyp:HDL concentration ratios (Fig. 7A). While hyp delivery in PBS and LDL is sufficiently visible in cancer cells 5 h after administrations, hyp in HDL enabled monitoring of cancer cells already in the first few hours after its administration. These results suggest that hyp can target cancer cells independently on LDL and HDL, but earlier cancer cells monitoring can be performed using HDL delivery. This could be the consequence of the faster release of hyp from HDL than LDL, which we described in this study. It should be noted that the hyp fluorescence intensities (directly proportional to therapeutic concentrations) detected in CAM 24 h after delivery were very similar. Representative hyp fluorescence images of SK BR 3 cancer cells grafted on CAM are shown in Fig. 7C. Intravenous administration of hyp:LDL and hyp:HDL may change the time of tumor targeting, and should be further investigated. The results obtained here represent valuable information that can be exploited in PDT dosimetry.

## 4. Conclusion

Progress in methods and approaches to improve anticancer treatments indicate that it is necessary to develop an appropriate transport system and PS with rational design to targeted cancer cells. LDL and HDL particles represent naturally-based transporters that can be very effective for hydrophobic/amphiphilic molecules delivery. We endeavored to point out the advantage and disadvantage of LDL and HDL applications as a transport system for hydrophobic molecules. In summary, our results demonstrated that both LDL and HDL could be effectively used for hyp transport and cancer cells targeting. If the concentration ratio between hyp (hydrophobic drug) and LDL is low (up to 10:1), hyp in LDL is specifically delivered into lysosomes of cancer cells *via* endocytosis. However, at shorter incubation times the therapeutically used intracellular concentration of hyp is low. Hyp concentration could be increased by longer incubation of cancer cells with hyp:LDL. At higher hyp:LDL concentration ratios (above 50:1), the delivery is less specific but hyp intracellular concentration is comparable to hyp alone, as it was observed in our previous publications [30,57]. In these publications, we have demonstrated, that hyp passed into the cells both by diffusion and endocytosis. Besides, we have also shown that intracellular concentration of hyp strongly depends on hyp:LDL ratio and significantly influences the PDT effect. For this reason, LDL is more suitable in applications where gradual release of hyp (hydrophobic molecules) is essential for the anticancer therapy. In the case of HDL the observed effects are similar as in LDL, but HDL particles released hyp easier than LDL. Our CAM studies point out that hyp:LDL, hyp:HDL and hyp biodistributions (hyp fluorescence intensities) are different during 3 h after their administration on CAM surface. However, hyp fluorescence detection after 24 h was in all studied cases the same. Drug-light interval in PDT is crucial. In the present study, the applied 1 h drug-light interval was not sufficient to acquire the same PDT effect for hyp:LDL, hyp:HDL and hyp. But, as we have previously reported, longer drug-light intervals could increase PDT effect in cancer cells, in such manner that hyp and hyp:LDL application result in the same PDT effects. Our results can provide strategies for the development of adequate targeted therapy.

## Conflict of interest

The Authors have no conflict of interest to declare.

## Acknowledgements

This work was funded by the Slovak Research and Development Agency VEGA1/0156/18, VEGA1/0421/18, VEGA2/0096/18, VEGA1/0929/16, and APVV-15-0485. The authors strongly appreciate this support.

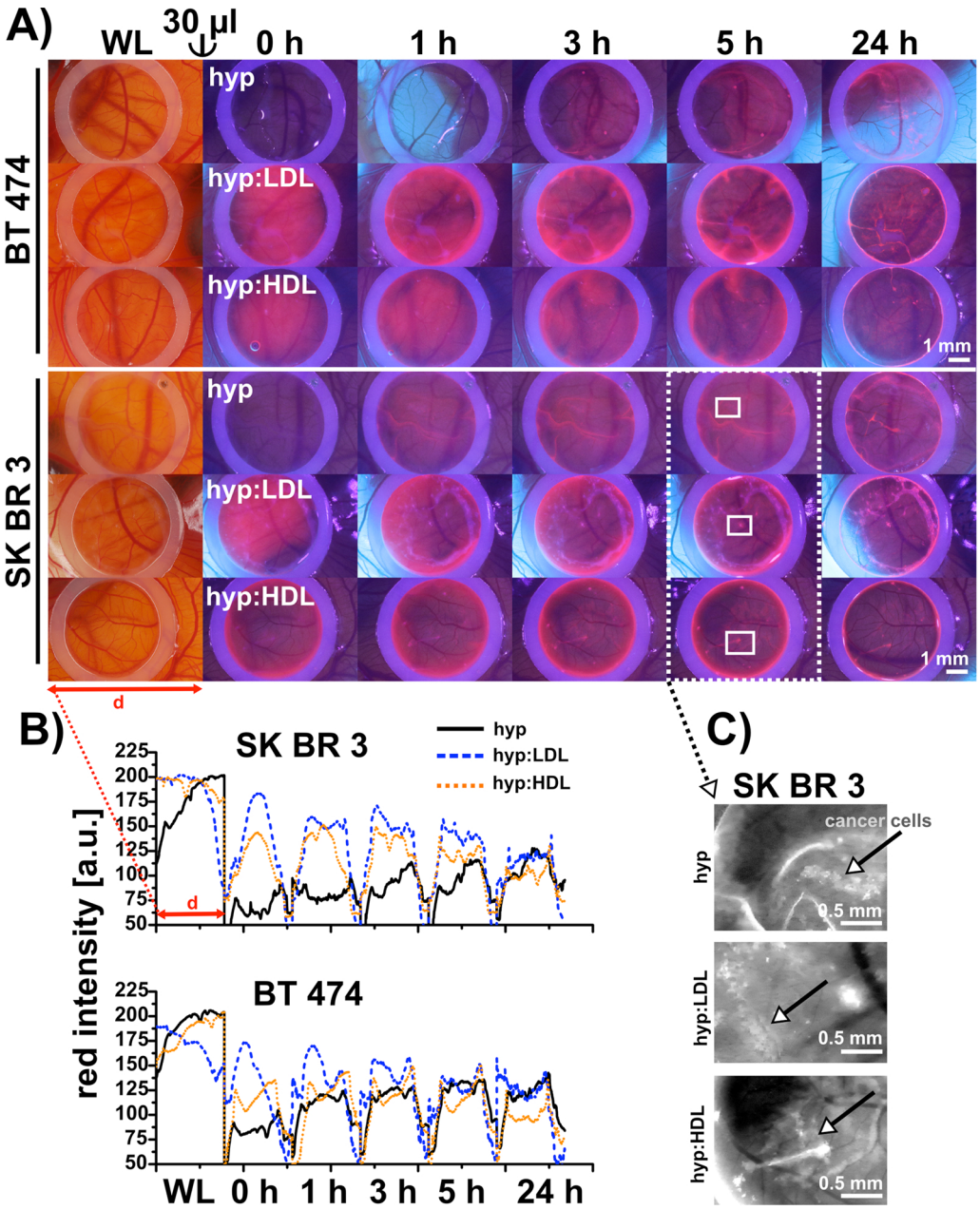


**Fig. 7.** A) Representative photos of hyp fluorescence on CAM and BT 474 and SK BR 3 cells seeded on CAM surface. 30 µl of hyp, hyp:LDL = 20:1 and hyp:HDL = 20:1 were topicaly applied to silicon circles defined areas. WL-white light detection. Hyp was excited with light emitted from 405 nm diodes. B) Plot profiles represent red intensity of RGB images as presented in A for CAMs with BT 474 and SK BR 3 cells: hyp (solid black line), hyp:LDL (dashed blue line) and hyp:HDL (dotted orange line); a red arrow (d) represents the width of the image. C) Zoomed areas of CAMs (white squares in A) with SK BR 3 cells 5 h after hyp, hyp:LDL and hyp:HDL administration. Black arrows point to SK BR 3 cells localization represented by hyp fluorescence (bright pixels).

## References


[1] M. Estanqueiro, M.H. Amaral, J. Conceicao, J.M.S. Lobo, Nanotechnological carriers for cancer chemotherapy: The state of the art, Colloids Surf. B-Biointerfaces 126 (2015) 631–648.

[2] A. Wicki, D. Witzigmann, V. Balasubramanian, J. Huwyler, Nanomedicine in cancer therapy: challenges, opportunities, and clinical applications, J. Control. Release 200 (2015) 138–157.

[3] X.Y. Xu, W. Ho, X.Q. Zhang, N. Bertrand, O. Farokhzad, Cancer nanomedicine: from targeted delivery to combination therapy, Trends Mol. Med. 21 (4) (2015) 223–232.

[4] A.P. Castano, T.N. Demidova, M.R. Hamblin, Mechanisms in photodynamic therapy: part one-photosensitizers, photochemistry and cellular localization, Photodiagnosis Photodyn. Ther. 1 (4) (2004) 279–293.

[5] S.B. Brown, E.A. Brown, I. Walker, The present and future role of photodynamic therapy in cancer treatment, Lancet Oncol. 5 (8) (2004) 497–508.

[6] V. Huntosova, G. Wagnieres, CHAPTER 15 pO2 measurements in biological tissues by luminescence lifetime spectroscopy: strategies to exploit or minimize phototoxic effects in tumors, quenched-phosphorescence detection of molecular oxygen: applications in life sciences, R. Soc. Chem. (2018) 298–318.

[7] P. Miskovsky, Hypericin–a new antiviral and antitumor photosensitizer: mechanism of action and interaction with biological macromolecules, Curr. Drug Targets 3 (1) (2002) 55–84.

[8] P. Agostinis, A. Vantieghem, W. Merlevede, P.A.M. de Witte, Hypericin in cancer treatment: more light on the way, Int. J. Biochem. Cell Biol. 34 (3) (2002) 221–241.

[9] T.A. Theodossiou, J.S. Hothersall, P.A. De Witte, A. Pantos, P. Agostinis, The multifaceted photocytotoxic profile of hypericin, Mol. Pharm. 6 (6) (2009) 1775–1789.

[10] A. Karioti, A.R. Bilia, Hypericins as potential leads for new therapeutics, Int. J. Mol. Sci. 11 (2) (2010) 562–594.

[11] B. Chen, Y. Xu, T. Roskams, E. Delaey, P. Agostinis, J.R. Vandenheede, P. de Witte, Efficacy of antitumoral photodynamic therapy with hypericin: Relationship between biodistribution and photodynamic effects in the RIF-1 mouse tumor model, Int. J. Cancer 93 (2) (2001) 275–282.

[12] V. Huntosova, K. Stroffekova, Hypericin in the dark: Foe or Ally in photodynamic therapy? Cancers (Basel) 8 (10) (2016).

[13] M. Misuth, J. Joniova, D. Horvath, L. Dzurova, Z. Nichtova, M. Novotova, P. Miskovsky, K. Stroffekova, V. Huntosova, The flashlights on a distinct role of protein kinase C delta: phosphorylation of regulatory and catalytic domain upon oxidative stress in glioma cells, Cell. Signal. 34 (2017) 11–22.

[14] A. Puri, K. Loomis, B. Smith, J.H. Lee, A. Yavlovich, E. Heldman, R. Blumenthal, Lipid-based nanoparticles as pharmaceutical drug carriers: from concepts to clinic, Crit. Rev. Ther. Drug Carrier Syst. 26 (6) (2009) 523–580.

[15] R. Savla, J. Browne, V. Plassat, K.M. Wasan, E.K. Wasan, Review and analysis of FDA approved drugs using lipid-based formulations, Drug Dev. Ind. Pharm. 43 (11) (2017) 1743–1758.

[16] P. Yingchoncharoen, D.S. Kalinowski, D.R. Richardson, Lipid-based drug delivery systems in cancer therapy: What is available and what is yet to come, Pharmacol. Rev. 68 (3) (2016) 701–787.

[17] G.I. Harisa, F.K. Alanazi, Low density lipoprotein bionanoparticles: from cholesterol transport to delivery of anti-cancer drugs, J. Saudi Pharm. Soc. 22 (6) (2014) 504–515.
[18] J.L. Goldstein, M.S. Brown, R.G. Anderson, D.W. Russell, W.J. Schneider, Receptor-mediated endocytosis: concepts emerging from the LDL receptor system, Annu. Rev. Cell Biol. 1 (1985) 1–39.
[19] M.S. Brown, J.L. Goldstein, Receptor-mediated control of cholesterol-metabolism, Science 191 (4223) (1976) 150–154.
[20] S. Vitols, C. Peterson, O. Larsson, P. Holm, B. Aberg, Elevated uptake of low-density lipoproteins by human lung-cancer tissue invivo, Cancer Res. 52 (22) (1992) 6244–6247.
[21] M.J. Rudling, B. Angelin, C.O. Peterson, V.P. Collins, Low density lipoprotein receptor activity in human intracranial tumors and its relation to the cholesterol requirement, Cancer Res. 50 (3) (1990) 483–487.
[22] J.B. German, J.T. Smilowitz, A.M. Zivkovic, Lipoproteins: when size really matters, Curr. Opin. Colloid Interface Sci. 11 (2-3) (2006) 171–183.
[23] A. Kader, A. Pater, Loading anticancer drugs into HDL as well as LDL has little affect on properties of complexes and enhances cytotoxicity to human carcinoma cells, J. Control. Release 80 (1-3) (2002) 29–44.
[24] C. Rohrl, H. Stangl, HDL endocytosis and resecretion, Biochim. Et Biophys. Acta-Mol. Cell Biol. Lipids 1831 (11) (2013) 1626–1633.
[25] D.E. Marotta, W.G. Cao, E.P. Wileyto, H. Li, I. Corbin, E. Rickter, J.D. Glickson, B. Chance, G. Zheng, T.M. Busch, Evaluation of bacteriochlorophyll-reconstituted low-density lipoprotein nanoparticles for photodynamic therapy efficacy in vivo, Nanomedicine 6 (3) (2011) 475–487.
[26] N.L. Andreazza, C. Vevert-Bizet, G. Bourg-Heckly, F. Sureau, M.J. Salvador, S. Bonneau, Berberine as a photosensitizing agent for antitumoral photodynamic therapy: Insights into its association to low density lipoproteins, Int. J. Pharm. 510 (1) (2016) 240–249.
[27] S. Bonneau, C. Vever-Bizet, H. Mojzisova, D. Brault, Tetrapyrrole-photosensitizers vectorization and plasma LDL: a physico-chemical approach, Int. J. Pharm. 344 (1-2) (2007) 78–87.
[28] J.C. Maziere, R. Santus, P. Morliere, J.P. Reyftmann, C. Candide, L. Mora, S. Salmon, C. Maziere, S. Gatt, L. Dubertret, Cellular uptake and photosensitizing properties of anticancer porphyrins in cell-membranes and low and high-density lipoproteins, J. Photochem. Photobiol. B-Biol. 6 (1-2) (1990) 61–68.
[29] B. Chen, B.W. Pogue, P.J. Hoopes, T. Hasan, Vascular and cellular targeting for photodynamic therapy, Crit. Rev. Eukaryot. Gene Expr. 16 (4) (2006) 279–305.
[30] V. Huntosova, Z. Nadova, L. Dzurova, V. Jakusova, F. Sureau, P. Miskovsky, Cell death response of U87 glioma cells on hypericin photoactivation is mediated by dynamics of hypericin subcellular distribution and its aggregation in cellular organelles, Photochem. Photobiol. Sci. 11 (9) (2012) 1428–1436.
[31] J. Dandler, B. Wilhelm, H. Scheer, Distribution of chlorophyll- and bacteriochlorophyll-derived photosensitizers in human blood plasma, Photochem. Photobiol. 86 (1) (2010) 182–193.
[32] B. Chauvin, B.I. Iorga, P. Chaminade, J.L. Paul, P. Maillard, P. Prognon, A. Kasselouri, Plasma distribution of tetraphenylporphyrin derivatives relevant for photodynamic therapy: importance and limits of hydrophobicity, Eur. J. Pharm. Biopharm. 83 (2) (2013) 244–252.
[33] L. Maletinska, E.A. Blakely, K.A. Bjornstad, D.F. Deen, L.J. Knoff, T.M. Forte, Human glioblastoma cell lines: levels of low-density lipoprotein receptor and low-density lipoprotein receptor-related protein, Cancer Res. 60 (8) (2000) 2300–2303.
[34] S.L. Gonias, N. Karimi-Mostowfi, S.S. Murray, E. Mantuano, A.S. Gilder, Expression of LDL receptor-related proteins (LRPs) in common solid malignancies correlates with patient survival, PLoS One 12 (10) (2017) e0186649.
[35] M. Alique, C. Luna, J. Carracedo, R. Ramirez, LDL biochemical modifications: a link between atherosclerosis and aging, Food Nutr. Res. 59 (2015) 29240.
[36] Y.Z. Wang, C. Wang, Y. Ding, J. Li, M. Li, X. Liang, J.P. Zhou, W. Wang, Biomimetic HDL nanoparticle mediated tumor targeted delivery of indocyanine green for enhanced photodynamic therapy, Colloids Surf. B-Biointerfaces 148 (2016) 533–540.
[37] V. Huntosova, D. Buzova, D. Petrovajova, P. Kasak, Z. Nadova, D. Jancura, F. Sureau, P. Miskovsky, Development of a new LDL-based transport system for hydrophobic/amphiphilic drug delivery to cancer cells, Int. J. Pharm. 436 (1-2) (2012) 463–471.
[38] V. Huntosova, K. Stroffekova, G. Wagnieres, M. Novotova, Z. Nichtova, P. Miskovsky, Endosomes: guardians against [Ru(Phen)(3)](2+) photo-action in endothelial cells during in vivo pO(2) detection? Metallomics 6 (12) (2014) 2279–2289.
[39] V. Huntosova, S. Gay, P. Nowak-Sliwinska, S.K. Rajendran, M. Zellweger, H. van den Bergh, G. Wagnieres, In vivo measurement of tissue oxygenation by time-resolved luminescence spectroscopy: advantageous properties of dichlorotris(1, 10-phenanthroline)-ruthenium(II) hydrate, J. Biomed. Opt. 19 (7) (2014) 77004.
[40] V. Huntosova, E. Gerelli, D. Horvath, G. Wagnieres, Measurement of pO(2) by luminescence lifetime spectroscopy: a comparative study of the phototoxicity and sensitivity of [Ru(Phen)(3)](2+) and PdTCPP in vivo, J. Biophotonics 10 (5) (2017) 708–717.
[41] M. Burikova, B. Bilcik, M. Macajova, P. Vyboh, J. Bizik, A. Mateasik, P. Miskovsky, I. Cavarga, Hypericin fluorescence kinetics in the presence of low density lipoproteins: study on quail CAM assay for topical delivery, Gen. Physiol. Biophys. 35 (2016) 459–468.
[42] I. Cavarga, B. Bilcik, P. Vyboh, M. Zaskvarova, D. Chorvat, P. Kasak, P. Mlkvy, A. Mateasik, A. Chorvatova, P. Miskovsky, Photodynamic effect of hypericin after topical application in the Ex Ovo quail chorioallantoic membrane model, Planta Med. 80 (1) (2014) 56–62.
[43] L. Blascakova, D. Horvath, D. Belej, G. Wagnieres, P. Miskovsky, D. Jancura, V. Huntosova, Hypericin cross barriers of the chicken's chorioallantoic membrane model when delivered in low-density lipoproteins, Photodiagnosis Photodyn. Ther. 23 (2018) 306–313.
[44] N. Leopold, B. Lendl, A new method for fast preparation of highly surface-enhanced Raman scattering (SERS) active silver colloids at room temperature by reduction of silver nitrate with hydroxylamine hydrochloride, J. Phys. Chem. B 107 (24) (2003) 5723–5727.
[45] R.F. Aroca, R.A. Alvarez-Puebla, N. Pieczonka, S. Sanchez-Cortez, J.V. Garcia-Ramos, Surface-enhanced Raman scattering on colloidal nanostructures, Adv. Colloid Interface Sci. 116 (1-3) (2005) 45–61.
[46] C.A. Schneider, W.S. Rasband, K.W. Eliceiri, NIH image to imageJ: 25 years of image analysis, Nat. Methods 9 (7) (2012) 671–675.
[47] S.W.E. van de Poll, T.C.B. Schut, A. van den Laarse, G.J. Puppels, In situ investigation of the chemical composition of ceroid in human atherosclerosis by Raman spectroscopy, J. Raman Spectrosc. 33 (7) (2002) 544–551.
[48] C. Stiebing, L. Schmolz, M. Wallert, C. Matthaus, S. Lorkowski, J. Popp, Raman imaging of macrophages incubated with triglyceride-enriched oxLDL visualizes translocation of lipids between endocytic vesicles and lipid droplets, J. Lipid Res. 58 (5) (2017) 876–883.
[49] K. Kneipp, H. Kneipp, I. Itzkan, R.R. Dasari, M.S. Feld, Ultrasensitive chemical analysis by Raman spectroscopy, Chem. Rev. 99 (10) (1999) 2957.
[50] S. Lin, L. Quaroni, W.S. White, T. Cotton, G. Chumanov, Localization of carotenoids in plasma low-density lipoproteins studied by surface-enhanced resonance Raman spectroscopy, Biopolymers 57 (4) (2000) 249–256.
[51] S. Schlucker, A. Szeghalmi, M. Schmitt, J. Popp, W. Kiefer, Density functional and vibrational spectroscopic analysis of beta-carotene, J. Raman Spectrosc. 34 (6) (2003) 413–419.
[52] S.C. Pinzaru, C. Muller, S. Tomsic, M.M. Venter, B.I. Cozar, B. Glamuzina, New SERS feature of -carotene: consequences for quantitative SERS analysis, J. Raman Spectrosc. 46 (7) (2015) 597–604.
[53] D. Krilov, M. Kosovic, M. Balarin, O. Gamulin, J. Brnjas-Kraljevic, Interaction of high density lipoprotein with nicotine - an IR and Raman study, Croat. Chem. Acta 83 (4) (2010) 387–393.
[54] G. Lajos, D. Jancura, P. Miskovsky, J.V. Garcia-Ramos, S. Sanchez-Cortes, Interaction of the photosensitizer Hypericin with low-density lipoproteins and phosphatidylcholine: a surface-enhanced Raman scattering and surface-enhanced fluorescence study, J. Phys. Chem. C 113 (17) (2009) 7147–7154.
[55] S. Kascakova, Z. Nadova, A. Mateasik, J. Mikes, V. Huntosova, M. Refregiers, F. Sureau, J.C. Maurizot, P. Miskovsky, D. Jancura, High level of low-density lipoprotein receptors enhance hypericin uptake by U-87 MG cells in the presence of LDL, Photochem. Photobiol. 84 (1) (2008) 120–127.
[56] A.P. Castano, T.N. Demidova, M.R. Hamblin, Mechanisms in photodynamic therapy: Part three- Photosensitizer pharmacokinetics, biodistribution, tumor localization and modes of tumor destruction, Photodiagnosis Photodyn. Ther. 2 (2) (2005) 91–106.
[57] V. Huntosova, L. Alvarez, L. Bryndzova, Z. Nadova, D. Jancura, L. Buriankova, S. Bonneau, D. Brault, P. Miskovsky, F. Sureau, Interaction dynamics of hypericin with low-density lipoproteins and U87-MG cells, Int. J. Pharm. 389 (1-2) (2010) 32–40.
[58] G. Bano, J. Stanicova, D. Jancura, J. Marek, M. Bano, J. Ulicny, A. Strejckova, P. Miskovsky, On the diffusion of Hypericin in dimethylsulfoxide/water mixtures-the effect of aggregation, J. Phys. Chem. B 115 (10) (2011) 2417–2423.
[59] S. Kascakova, M. Refregiers, D. Jancura, F. Sureau, J.C. Maurizot, P. Miskovsky, Fluorescence spectroscopic study of hypericin-photosensitized oxidation of low-density lipoproteins, Photochem. Photobiol. 81 (6) (2005) 1395–1403.
[60] P. Gbur, R. Dedic, D. Chorvat, P. Miskovsky, J. Hala, D. Jancura, Time-resolved luminescence and singlet oxygen formation after illumination of the Hypericin-low-density lipoprotein complex, Photochem. Photobiol. 85 (3) (2009) 816–823.
[61] P. Mukherjee, R. Adhikary, M. Halder, J.W. Petrich, P. Miskovsky, Accumulation and interaction of hypericin in low-density lipoprotein–a photophysical study, Photochem. Photobiol. 84 (3) (2008) 706–712.
[62] B.A. Allison, P.H. Pritchard, J.G. Levy, Evidence for low-density lipoprotein receptor-mediated uptake of benzoporphyrin derivative, Br. J. Cancer 69 (5) (1994) 833–839.
[63] S.C. Whitman, A. Daugherty, S.R. Post, Regulation of acetylated low density lipoprotein uptake in macrophages by pertussis toxin-sensitive G proteins, J. Lipid Res. 41 (5) (2000) 807–813.
[64] R.E. Pitas, Expression of the acetyl low density lipoprotein receptor by rabbit fibroblasts and smooth muscle cells. Up-regulation by phorbol esters, J. Biol. Chem. 265 (21) (1990) 12722–12727.
[65] V. Verebova, D. Belej, J. Joniova, Z. Jurasekova, P. Miskovsky, T. Kozar, D. Horvath, J. Stanicova, V. Huntosova, Deeper insights into the drug defense of glioma cells against hydrophobic molecules, Int. J. Pharm. 503 (1-2) (2016) 56–67.
[66] A.P. Castano, T.N. Demidova, M.R. Hamblin, Mechanisms in photodynamic therapy: part two-cellular signaling, cell metabolism and modes of cell death, Photodiagnosis Photodyn. Ther. 2 (1) (2005) 1–23.
[67] H. Zhao, R. Yin, Y. Wang, Y.H. Lee, T. Luo, J. Zhang, H. Qiu, S. Ambrose, L. Wang, J. Ren, J. Yao, D. Chen, Z. Liang, J. Zhen, S. Wu, Z. Ye, J. Zeng, N. Huang, Y. Gu, Modulating mitochondrial morphology enhances antitumor effect of 5-ALA-mediated photodynamic therapy both in vitro and in vivo, J. Photochem. Photobiol. B 176 (2017) 81–91.
[68] W.P. Hu, K.K. Kuo, G.C. Senadi, L.S. Chang, J.J. Wang, Photodynamic therapy using indolines-fused-triazoles induces mitochondrial apoptosis in human non-melanoma BCC Cells, Anticancer Res. 37 (10) (2017) 5499–5505.
[69] J.J. Reiners Jr., P. Agostinis, K. Berg, N.L. Oleinick, D. Kessel, Assessing autophagy in the context of photodynamic therapy, Autophagy 6 (1) (2010) 7–18.
[70] O.J. Norum, P.K. Selbo, A. Weyergang, K.E. Giercksky, K. Berg, Photochemical

internalization (PCI) in cancer therapy: from bench towards bedside medicine, J. Photochem. Photobiol. B 96 (2) (2009) 83–92.
[71] A. Weyergang, O. Kaalhus, K. Berg, Photodynamic therapy with an endocytically located photosensitizer cause a rapid activation of the mitogen-activated protein kinases extracellular signal-regulated kinase, p38, and c-Jun NH2 terminal kinase with opposing effects on cell survival, Mol. Cancer Ther. 7 (6) (2008) 1740–1750.
[72] L.B. Sicchieri, A.M. Monteiro, R.E. Samad, A.S. Ito, A.M.F. Neto, N.D. Vieira J., M. Gidlund, L.C. Courrol, Study of tryptophan lifetime fluorescence following low-density lipoprotein modification, Appl. Spectrosc. 67 (4) (2013) 379–384.